

Catalysis Science & Technology

Accepted Manuscript

This article can be cited before page numbers have been issued, to do this please use: O. Gomez-Capiro, L. Bravo, P. Lagos, P. Santander, G. Pecchi and A. Karelavic, *Catal. Sci. Technol.*, 2021, DOI: 10.1039/D1CY01060C.



This is an Accepted Manuscript, which has been through the Royal Society of Chemistry peer review process and has been accepted for publication.

Accepted Manuscripts are published online shortly after acceptance, before technical editing, formatting and proof reading. Using this free service, authors can make their results available to the community, in citable form, before we publish the edited article. We will replace this Accepted Manuscript with the edited and formatted Advance Article as soon as it is available.

You can find more information about Accepted Manuscripts in the [Information for Authors](#).

Please note that technical editing may introduce minor changes to the text and/or graphics, which may alter content. The journal's standard [Terms & Conditions](#) and the [Ethical guidelines](#) still apply. In no event shall the Royal Society of Chemistry be held responsible for any errors or omissions in this Accepted Manuscript or any consequences arising from the use of any information it contains.

Kinetic and structural understanding of bulk and supported vanadium-based catalysts for furfural oxidation to maleic anhydride†

View Article Online
DOI: 10.1039/D1CY01060C

Received 00th January 20xx,
Accepted 00th January 20xx

DOI: 10.1039/x0xx00000x

Oscar Gómez-Cápiro^{a,b}, Luis Bravo^a, Patricio Lagos^a, Paola Santander^{a,b}, Gina Pecchi^{b,c}, Alejandro Karelovic^{a,b,d}

The kinetics of gas-phase furfural partial oxidation to maleic anhydride (MA) was studied over bulk vanadium-phosphorous-based catalysts obtained by aqueous (VPAq) and organic (VPOr) methods and compared to a supported V_2O_5/Al_2O_3 catalyst. The solids were characterized by N_2 adsorption-desorption, XRD and UV-vis DRS. Results showed a higher specific surface area on VPOr compared with VPAq materials, with a well-defined $(VO)_2P_2O_7$ crystalline structure. UV-vis analysis showed mainly V(V) on VPAq and an intermediate state between V(IV)-V(V) on VPOr. A detailed kinetic study demonstrated that furfural can be oxidized to MA or CO_x through parallel paths. At high oxygen partial pressures MA oxidation is inhibited on VPO catalysts but favored on V_2O_5/Al_2O_3 . A Langmuir-Hinshelwood kinetic model with negligible sites occupancy fits the experimental data with a 16% mean error. It also shows a higher apparent activation energy for furfural partial oxidation than for complete oxidation highlighting the favored selectivity to maleic anhydride at higher temperatures on VPO catalysts.

Introduction.

Maleic Anhydride (MA) is used as raw material for the production of resins, agrochemicals, and coatings ^{1,2}. It is currently produced from the partial oxidation of petrochemicals, mainly n-butane ³⁻⁵. The n-butane partial oxidation has been extensively studied in terms of reaction conditions ^{6,7}, catalysts structure dependence ⁸⁻¹⁰, promoters and selectivity to maleic anhydride ^{11,12}, and kinetics ¹³⁻¹⁶. However, the possibility of obtaining MA by similar reactions from furfural ¹⁷ has been little investigated. The use of furfural obtained from biomass ¹⁸⁻²⁰ contributes to reducing the carbon footprint of the products that use MA as raw material, hence it is a real possibility to join biorefineries with current technologies in the chemical industry. The furfural partial oxidation in the aqueous phase has been studied always in batch process ²¹⁻²⁵. However, continuous processes are more efficient and have a better chance of becoming commercially established ²⁶. In this sense, furfural partial oxidation in gas phase presents a clear advantage, which is not free of obstacles. One of the main limitations of this alternative is the formation of polymerization products under the normally used reaction conditions (240°C-360°C) ²⁷.

Catalysts based on vanadium are the most used for partial oxidation of organic molecules, reported as supported and bulk catalysis ^{24,27,28}. It has been reported that furfural partial oxidation reaction proceeds

through the so-called redox Mars-van Krevelen (MvK) mechanism ²⁹. In this mechanism, the structure of the catalyst and the nature of the support have a strong influence on the catalytic activity ^{30,31}. According to their location in the solid, the O atoms have different probabilities of reacting ³². However, the oxidation states of V are not equally active, being V(IV) the most selective to the formation of MA ³⁰. The oxidation state of the V phase is strongly affected by the nature of the precursor, preparation method and thermal treatment after the synthesis of the catalysts. Consequently, calcination temperature and media (air, O_2 , N_2 , etc.) are parameters to be taken into account during the synthesis ^{33,34}. Additionally, it has been reported that the nature of the solvent, aqueous or organic, has a strong influence on the crystalline structure obtained after the activation of the catalyst ^{8,35} that define the activity and selectivity towards MA ^{29,36,37}. It has been also reported that, even though P do not catalyse the MA formation ²³, it improves the thermal resistance of the solids ³⁸ and limits the total oxidation of the surface V atoms, maintaining the selectivity to MA ³⁹. Several authors reported $(VO)_2P_2O_7$ phase as the most active to the selective partial furfural oxidation towards MA ^{35,36,40}, being detected by X-ray diffraction (XRD), UV-vis diffuse reflectance spectroscopy, Raman spectroscopy, among others ^{28,41}.

Kinetic models of partial catalytic oxidation reactions over metal transition oxides catalysts has been developed mostly for n-butane as raw material ^{4,5,42,43}. There is a consensus that the oxygen involved in the reaction is provided by the support ^{10,15,27}. In the case of oxidation of n-butane to MA over partially reduced vanadyl pyrophosphate catalysts, it has been reported that the catalyst reoxidation step displays a reaction order of 0.55 with respect to the oxygen pressure, in a range of 2.1 and 21 %vol. O_2 and 345°C to 400°C, implying dissociative O_2 adsorption under the experimental conditions ⁴⁴. On the other hand, Murthy and Rajamani studied vanadium pentoxide catalysts for furfural partial oxidation to MA.

^a Carbon and Catalysis Laboratory (CarboCat), Department of Chemical Engineering, University of Concepción, Concepción, Chile.

^b Millennium Nuclei on Catalytic Process towards Sustainable Chemistry (CSC), Chile.

^c Physical Chemistry Department, Faculty of Chemical Sciences, University of Concepción, Chile.

^d Unidad de Desarrollo Tecnológico (UDT), Universidad de Concepción, Chile.

* Corresponding author akarelov@udec.cl (A. Karelovic)

† Electronic Supplementary Information (ESI) available. See DOI: 10.1039/x0xx00000x

ARTICLE

Catalysis Science & Technology

They proposed a two-stage redox mechanism with a first reaction order to furfural and oxygen partial pressure, in the range 200–280°C⁴⁵. The same authors suggested the re-oxidation of the support as the rate-determining step under the experimental conditions of the study⁴⁶. Regarding supported VO_x catalysts, Alonso-Fagundez et al. report a Langmuir-Hinshelwood model with first-order reaction for both furfural and O₂ based on experimental results²⁹.

In this work, we report the effect of the nature of the preparation method (aqueous or organic) and the P/V molar ratio in the structure of V-P-O catalysts to be used in the gas phase partial oxidation of furfural to maleic anhydride. We performed a kinetic study varying the residence time, temperature and P_{O₂}/P_{furf} feed ratio. A model developed using a simplified Langmuir-Hinshelwood formalism assuming O₂ molecular dissociation and second O atom addition as the rate determining steps for both total and selective oxidation, fitted the experimental data with a mean error of 16.3%. We also present the kinetic parameters obtained for V₂O₅/Al₂O₃ for comparison, and show the higher activity of the latter catalyst, for both selective and unselective paths, highlighting the suitability of VPO catalysts at higher oxidizing conditions. Additionally, the negligible coverage predicted by the model shows that the reactions present apparent first-order kinetics.

Experimental.

Catalysts preparation.

Catalysts were prepared using two methods, one based on aqueous (VPAq) and the other on organic (VPOr) medium. It is well known that both methods allow obtaining solids with marked structural and morphological differences, whose influence, although studied in the oxidation of n-butane, has not been studied in depth in the selective oxidation of furfural. For the VPAq method⁴⁷, three catalysts with a nominal P/V molar ratio of 0.43, 0.85, 1.0 were prepared. The most validated selective phase for n-butane selective oxidation to MA is the (VO)₂P₂O₇^{8,37,48}, which has a P/V molar ratio of 1.0, however, as this work deals with furfural instead of n-butane, we studied different P/V molar ratios to determine its impact on selectivity to MA. The procedure required 25 mL of distilled water heated at 60°C, H₃PO₄ (99% purity, Merck) added according to the nominal P/V molar ratio and 2.89 g of NH₄VO₃(s) (99% purity, Merck), as V source, mixed slowly, while the solution was kept at 400 rpm for 2h. This method was previously described by several authors^{40,47}. The dissolution was concentrated by rota-evaporation for 6h and the precursor dried at 105°C for 8h. The calcination was performed in a tubular reactor inside a cylindrical furnace at 500°C for 4h, with a heating rate of 2°C/min under a constant flow (40 mL/min) of N₂ (99.999% purity, Air Liquide).

For the VPOr organic phase method⁴⁹, the same nominal P/V molar ratios were used in isobutanol (14.1 mL) as the dissolution medium. V₂O₅ (1.18 g) obtained by the calcination of NH₄VO₃(s) (99% purity, Merck) was added with the appropriate amount of H₃PO₄ (99% purity, Merck). The dissolution was kept in a reflux heating at 110°C for 6h until a sky-blue color solid was obtained. The reaction products were filtered and washed with isobutanol and acetone according to

the method described previously⁵⁰. The obtained solids were dried and calcined as described before. Both series of VPOr and VPAq catalysts were ground to procure a particle size between 150 and 380 μm.

For a better comparison of the catalytic performance of the VPAq and VPOr catalysts, a supported V₂O₅/γ-Al₂O₃ catalyst was also studied, as it has been shown to be active for this reaction^{27,29,31}. We used a 21 wt.% V₂O₅/γ-Al₂O₃ (ca. 12 wt.% V) catalyst synthesized in our last work³¹. Briefly, the synthesis procedure was as follows: γ-Al₂O₃ (Saint-Gobain Norpro SA 6173) was impregnated with NH₄VO₃ in presence of oxalic acid (oxalic acid/NH₄VO₃ molar ratio of 2) in distilled water at 80°C under continuous stirring at 700 rpm. The metavanadate was gradually added until a dark blue dissolution was obtained and, once the oxalate-vanadium complex was formed, the dissolution under agitation was cooled down to room temperature. Finally, the dissolution was mixed with the support and dried under vacuum in a rotary evaporator at 58°C for 2 h. The solid as obtained was dried overnight at 105°C and calcined in static air at 500°C for 3 h using a heating rate of 10 °C/min.

Catalysts characterization

Adsorption-desorption of N₂ at 77K was used to analyze the morphological structure of the solids. A Tristar II 3020 (Micromeritics) device was used. After degassing under vacuum at 200°C for 4 h, the samples were analyzed to get the adsorption and desorption isotherms, following the suggestions of De Lange *et al.* for sample preparation and analysis⁵¹. The obtained data were processed using the BET⁵² model to estimate the specific surface and the BJH method⁵³ or the hydraulic radii using the Gurvitsch rule to obtain the pore volume^{54,55}. Elemental surface distribution of V and P was observed through Scanning Electron Microscopy-Energy Dispersive Spectroscopy technique using an EOL JSM-6610LV 6610LV (BES detector) device at an acceleration voltage of 20 kV. Samples were coated with a thin layer of gold for 30 s at 0.06 mbar using a DENTON VACUUM apparatus. The crystalline structure was analyzed by X-ray diffraction using a Bruker Endeavor D4 diffractometer with CuKα radiation (λ=0.154059 nm) using 0.02°/step and 1 s/step between 3° and 90°. Particle size and d-spacing were calculated according to the Scherrer equation (Eq. 1) and Bragg correlation (Eq. 2), respectively:

$$L = \frac{K\lambda}{\beta \cos(\theta)} \quad (1)$$

$$n\lambda = 2d \sin(\theta) \quad (2)$$

Where *L* is the particle size (nm), *K* is a constant equal to 0.94 for all solids, λ is the wavelength (nm), β is the full width at half-maximum intensity (FWHM) (°), θ is the plane angle (°), *n* is the order of reflection and *d* is the interplanar spacing (nm).

A Thermo Scientific Evolution 260 Bio spectrometer equipped with a Spectralon-coated integrating sphere ISA 220 was used to perform UV-vis diffuse reflectance spectroscopy (DRS). The spectra were recorded in the range of 190 and 1100 nm using a Spectralon disc as standard.

Catalytic tests.

Catalysts were tested at three temperatures (280°C, 300°C and 320°C) in a tubular reactor heated by a furnace controlled by an Omega CN7200 device and the gas flow was controlled by mass flow controllers (Kofloc D8500). We used a 3/8" diameter stainless steel reactor in which the catalysts was loaded sandwiched by quartz wool. The catalyst (40 mg) was mixed with quartz sand (400 mg) in order to prevent the formation of hotspots due to the exothermic nature of oxidation reactions. Before each experiment, the catalysts were activated using synthetic air at 350°C for 1h heating at 10°C/min. After that, the furfural/O₂/N₂ flow was introduced to the system and the temperature descended to 320°C to start the reaction at the highest temperature as suggest previous reports²⁷. Afterward, to check a deactivation process, the temperature was decreased to 300°C, then to 280°C, and finally increased to 320°C. Each temperature was maintained for 4 h. Furfural (Merck-Millipore) was fed using a saturator kept at 30°C in a thermostated bath, with the constant bubbling of 5 mL/min of N₂ to reach a partial pressure of 0.0804 kPa. The parameters, in the first round of experiments, were: P_{O₂}/P_{fur} ratio=20 (Synthetic Air, Air Liquide), 2 mL/min of Ar (99.999% purity, Air Liquide) as an internal reference, and N₂ (99.999% purity, Air Liquide) to complete a total flow of 22 mL/min. As a detector, a mass spectrometer device was used (Thermostar Omnistar GSD 320). The furfural conversion was determined according to equation 3 (Eq. 3). The equations 4 and 5 (Eq. 4 and Eq. 5) were used to calculate the yield (for MA and CO₂) and the space-time yield (STY) (for MA).

$$x_{fur} = \frac{P_{fur}^0 - P_{fur}}{P_{fur}^0} 100 \quad (3)$$

$$Y_i = \frac{\dot{n}_i}{a_i \dot{n}_{fur}^0} 100 \quad (4)$$

$$STY = \frac{\dot{m}_{MA}}{m_{cat}} \quad (5)$$

Where x_{fur} is the furfural conversion, P_{fur}^0 is the initial partial pressure of furfural, P_{fur} is the furfural partial pressure at the exhaust, Y_i is the yield of the product i , \dot{n}_i represent the molar flow of the product i in the exhaust, a_i represent the stoichiometric coefficient of product i (stoichiometric coefficient of furfural is one for all reactions), \dot{n}_{fur}^0 represent the initial molar flow of furfural, \dot{m}_{MA} is the MA mass flow in the exhaust and m_{cat} is the mass of the catalyst bed inside the reactor.

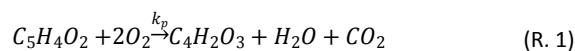
Once the performance of the catalysts was established, the VPOr_{1.0} and the V₂O₅/γ-Al₂O₃ catalysts were used in further analysis to perform a detailed kinetic study, changing the P_{O₂}/P_{fur} ratio, residence time (W/F ratio) and reaction temperature. Therefore, the P_{O₂}/P_{fur} ratios of 10, 20 and 40 were studied, and the W/F ratio was changed keeping constant the amount of catalyst, using total flows of 10, 30, and 40 mL/min, in addition to the 22 mL/min previously mentioned. The reagents and reaction products were analyzed inline with a GC (SRI 8610C) with a capillary column (30m x 0.53mm I.D. 1.0U MXT-WAX, Restek 70655-273) and three packed columns (6' x 1/8" Molecular sieve 5A, 18" x 1/8" Hayesep D and 6' x 1/8" Hayesep D). The system was equipped with a thermal conductivity detector (TCD), a flame ionization detector (FID) and a FID detector equipped with a methanizer.

Kinetic modeling of furfural partial oxidation.

View Article Online

DOI: 10.1039/D1CY01060C

The experimental data were used to fit a kinetic model to a simplified reaction scheme, with partial oxidation of furfural towards MA (R. 1), complete oxidation in a parallel reaction (R. 2) and subsequently the total oxidation of MA (R. 3).



As will be shown in section 3.5, the total oxidation of MA (R.3) was negligible for V-P-O catalysts, therefore the model was simplified to two main reactions (R.1 and R.2). To these simplified models, a Langmuir-Hinshelwood based model was studied. A 1-D pseudo-homogeneous model was assumed for the fixed bed reactor (Eq. 6), that was operated at integral conditions.

$$\frac{dP_i}{dW} = \frac{RT}{v} r_i \quad (6)$$

Where P_i is the partial pressure for compound i (kPa), W is the catalyst bed mass (g), R is the universal gas constant (J mol⁻¹ K⁻¹), T is the temperature (K), v is the volumetric flow rate of feed (ml min⁻¹) and r is the net reaction rate for the compound i (mol min⁻¹ g_{cat}⁻¹).

The absence of mass transfer limitations was checked using the recommended criteria (Section S1 of Supplementary Information). An optimization method based on genetic algorithms, using the optimization toolbox of Matlab®, was used to determine the model parameters, by minimizing the error between the experimental and calculated data. The objective function and method of calculation are detailed in Section S3.

Results and Discussion.

Morphological and elemental characteristics.

The VPAq and VPOr catalysts with different P/V molar ratios were characterized using N₂ adsorption-desorption isotherms at 77K (Figure S1 in Supplementary Information). The isotherms were classified as type II according to the IUPAC classification⁵⁶, typically of solid with low porosity or macro-porosity. Figure 1 shows the specific surface area as a function of the P/V molar ratio for the synthesized catalysts, and Table S3 summarizes the specific surface and the mean pore size values. It can be seen for VPOr and VPAq catalysts the same trend reported by Horowitz⁴⁰ i.e., a decrease in the surface area while increase the P/V molar ratio. Concerning the effect of the preparation method, VPOr catalysts presented higher surface area than VPAq, in all of the studied range of P/V molar ratio.

Although the specific surface area values are very low and may be within the error range of the measuring device, the differences between the two groups of catalysts are clear. Since all measurements were performed on the same device under similar environmental conditions, the differences between VPAq and VPOr can be assumed as significant. The pore volume in the VPAq group

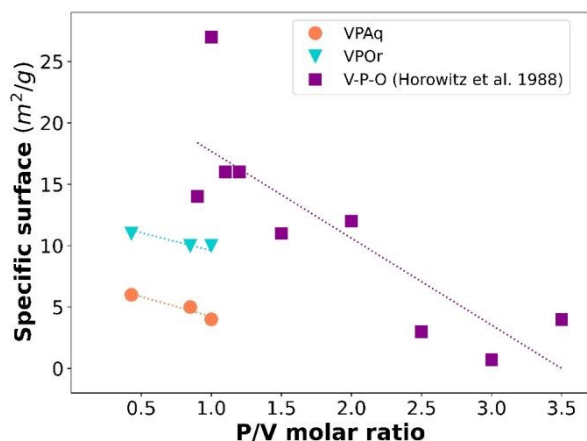


Figure 1. The specific surface area as a function of the P/V molar ratio for VPAq and VPOr ($P/V=0.43, 0.85, 1.00$). Data for V-P-O catalysts reported by Horowitz⁴⁰ is included. The lines are added to show the trend.

maintains the same tendency to decrease as the P/V ratio increases. However, this morphological parameter in the VPOr group shows an opposite behavior. On the other hand, the supported V_2O_5/Al_2O_3 catalyst presents high specific surface area ($158\text{ m}^2/\text{g}$), whereas showing a decrease of 30% of the initial $\gamma\text{-Al}_2O_3$ specific surface area ($227\text{ m}^2/\text{g}$) upon vanadium impregnation. The V_2O_5/Al_2O_3 and $\gamma\text{-Al}_2O_3$ isotherms and their pore size distribution are shown in Figure S1.

The elements distribution on the bulk catalysts surface were studied using SEM-EDS mapping. Figure S2 show the screenshots corresponding to each element founded in the catalysts. It is observed an homogeneous distribution in all catalysts, which is important to form V-P phases declared as active for organic molecules oxidation³⁰. In addition, Table 1 show the elemental composition determined by this technique. The V diminish as well the P increase observed into each catalysts group correspond with the changes expected according P/V molar ratio, although it may not represent the elemental composition of every solid.

Table 1. Elemental composition of VPAq and VPOr catalysts obtained by SEM-EDS analysis.

Catalyst	Elements (wt. %)		
	V	P	O
VPAq _{0.43}	43.28	17.95	38.75
VPAq _{0.85}	42.39	21.2	36.4
VPAq _{1.0}	41.6	21.92	36.48
VPOr _{0.43}	46.79	18.13	35.08
VPOr _{0.85}	42.55	20.28	37.17
VPOr _{1.0}	39.76	21.75	38.49

Crystalline structure.

View Article Online
DOI: 10.1039/D1CY01060C

Figure 2 shows the X-ray diffraction patterns associated with the crystalline structure of the synthesized catalysts. The observed features correspond to phases previously described^{35,57–59}, and it is observed that for higher P/V molar ratios VPOr catalysts display notorious diffraction peaks, indicative of more crystalline structures. On the contrary, VPAq catalysts are mainly amorphous. The differ-

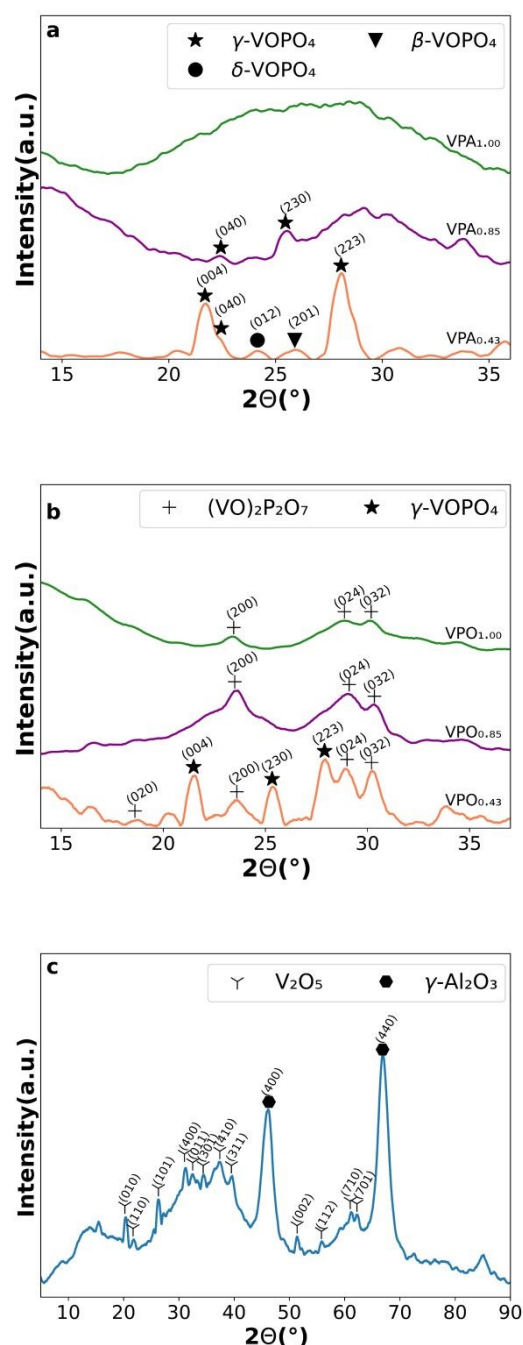


Figure 2. XRD patterns for (a) VPAq and (b) VPOr catalysts ($P/V=0.43, 0.85, 1.00$), and (c) V_2O_5/Al_2O_3 supported catalyst.

nce observed between both groups of catalysts coincide with previous results reported by Batis *et al.*⁵⁷, who prepared V-P-O catalysts by similar synthesis methods as used in this work. In the latter group of catalysts, VPAq_{0.43} catalyst show significant diffraction peaks (Fig. 2a) which correspond to VOPO₄ compounds, mainly γ -VOPO₄. In the case of VPAq_{0.85}, the plane (040) is maintained, and a new peak, attributed to γ -VOPO₄ (plane (230)) was identified⁵⁷. Regarding VPOr catalysts (Fig. 2b), the main difference with respect to the aqueous route of preparation is the appearance of (VO)₂P₂O₇ signals coexisting with γ -VOPO₄ in the case of VPOr_{0.43}. The (VO)₂P₂O₇ phase has been reported as the active catalytic phase for n-butane partial oxidation specifically the plane (200)^{8,37,48}, which is not detected in the VPAq catalysts. However, the evidence regarding the activity of this phase is much more scarce⁵⁹. These authors achieved high MA selectivities and yields, which is the focus of most studies in the field to the detriment of elucidating the kinetics governing the reaction.

The crystallite size, consistent with the planes (200), (032) and (024), corresponding to (VO)₂P₂O₇, were calculated by Scherrer equation and are shown in Table 2 for VPOr catalysts, together with the changes in the d-spacing related with the P/V molar ratio. The P-induced defects cause changes in the interplanar distance since the d-spacing increases progressively with the P/V molar ratio on plane (024) while it is still constant for plane (032). It has been reported d-spacing dimensions of 0.387 nm, 0.314 nm, and 0.298 nm for the planes (200), (024), and (032), respectively³⁷. The results show a minimum in the planes (200) and (024) (0.371nm and 0.301 nm) for VPOr_{0.85}. This means that increasing P concentration affects differently the (VO)₂P₂O₇ crystallite formation, favoring the growth in the direction of one plane over the others. Regarding the V₂O₅/Al₂O₃ pattern, only the peaks attributed to the crystalline V₂O₅ phase⁶⁰ and the support⁶¹ were detected (Fig. 2c).

These kind of patterns (Fig. 2a and 2b), with inhomogeneous line broadening of the diffraction lines of a crystalline phase, should not be analyzed with the Williamson-Hall methods because would provide wrong results⁶². Others authors use Scherrer equation to estimate the crystallite size of V-P-O catalysts with similar XRD patterns⁶³⁻⁶⁹.

Table 2. Crystallite particle size calculated by Scherrer equation, and d-spacing from Bragg correlation for different (VO)₂P₂O₇ planes for the VPOr catalysts.

P/V molar ratio	Particle size (nm) d-spacing (nm)		
	Plane (200)	Plane (024)	Plane (032)
0.43	22.0 0.372	17.9 0.302	14.9 0.291
0.85	14.7 0.371	8.9 0.301	14.9 0.290
1.00	14.7 0.375	8.9 0.307	22.4 0.290

UV-vis DRS and band gap energy determination.

View Article Online

DOI: 10.1039/D1CY01060C

UV-vis DRS experiments were carried out for a better understanding of the oxidation state of vanadium in the VPOr and VPAq catalysts (Fig. S3). The maximum of the main peak is presented in Table 3. Martin *et al.* reported a charge transfer transition band for V(IV) at 220 nm and the corresponding V(V) at 280 nm and 340-350 nm⁷⁰. The spectra indicate that the main peaks of the VPOr catalysts (243-256 nm) are closer to 220 nm than the VPAq signals (260 to 280 nm). This result is in line with XRD, which showed that (VO)₂P₂O₇, with V(IV) is the predominant crystalline phase in the VPOr catalysts. The shift towards higher wavelength for VPOr indicates an amorphous phase not identified by XRD with V(V) in its structure since the influence of γ -VOPO₄ (with V(V)) is negligible as P/V molar ratio increases, as show in the XRD pattern for these catalysts (Fig. 2b).

Table 3. The wavelength of the main peak of DRS as a function of the P/V molar ratio for the VPAq and VPO catalysts.

P/V molar ratio	VPAq Peak (nm)	VPOr Peak (nm)
0.43	280	243
0.85	275	256
1.00	260	252

The amorphous phase with V(V) is also evidenced for the VPAq where the wavelength values shifted towards 280 nm. Wavelength where the DRS maximum occurs (280 nm) for VPAq_{0.43} matches exactly with literature reports for pure V(V) phases⁷⁰. This was to be expected since this catalyst presents exclusively crystalline phases of vanadium phosphates (β -VOPO₄, δ -VOPO₄ and γ -VOPO₄). VPAq catalysts with P/V \geq 0.85 display a larger amount of amorphous phase with a large amount of V(V) species, but with presence of V(IV) as well, since the wavelength values are lower than 280 nm. The phase responsible for the decrease in the wavelength for the maximum in the DRS of VPAq catalysts with P/V \geq 0.85 could be a disorganized no crystalline structure of (VO)₂P₂O₇, impossible to detect in XRD analysis⁵⁷.

Determination of the catalytic activity of VPAq and VPOr.

The catalytic performance of VPAq and VPOr catalysts for the oxidation of furfural, was studied in the range of 280°C and 320°C. Figure 3 shows the MA yield as a function of the furfural conversion over the VPAq and VPOr catalysts. As expected, the increase in the reaction temperature produces an augmentation in the furfural conversion. Thus, as more furfural is converted, MA yield proportionally increases, with similar behavior regardless of the P/V molar ratio or the catalyst preparation method. The continuous increase in the MA yield with furfural conversion means that, even at the highest conversion rates (30-40%), MA does not suffer significant further oxidation reactions over the bulk catalysts. On the other hand, Figure 4 shows that for VPAq catalysts a decrease in the furfu-

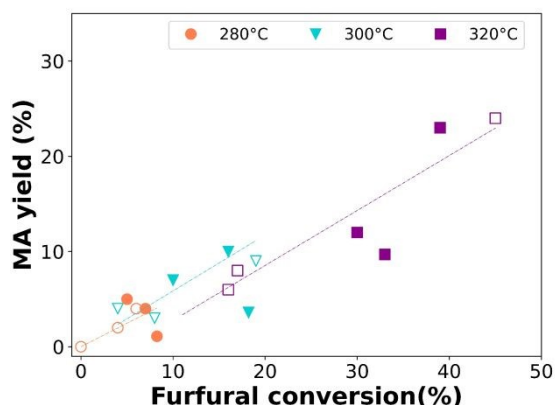


Figure 3. MA yield vs. Furfural conversion over VPAq (empty symbols) and VPOr (filled symbols) catalysts. (P/V molar ratios=0.43, 0.85, 1.00; $T=280^{\circ}\text{C}$, 300°C , 320°C ; $W/F=1.81$ min $\text{mg}_{\text{cat}} \text{mL}^{-1}$; $P_{\text{O}_2}/P_{\text{fur}}=20$). The lines are added to show the trend.

ral conversion is observed with the increase in the P/V molar ratio, whereas no significant effect is observed for VPOr catalysts.

Considering the previous characterization results, the lower furfural conversion for the VPAq catalysts can be attributed to their lower specific surface area (Fig. 1) and/or their lower crystallinity (Fig. 2a). Even taking into account that the specific surface areas of both groups of catalysts are low and that the crystallinity is not completely defined, it can be observed that the VPOr have a higher surface area for all the P/V ratios, while the VPAq do not show signs of the phase $(\text{VO})_2\text{P}_2\text{O}_7$ in the XRD patterns.

Evidence of that is the high furfural partial oxidation activity and MA yield of VPAq_{0.43} catalyst (Fig. 4a), which has the higher specific surface area and the best defined crystalline structure in the group of VPAq. These results suggests a combined effect of both crystalline structure and specific surface area on the improvement of the catalysts activity. A similar behaviour shows the VPOr_{0.43} catalyst, which has the highest specific surface area and the best-defined $(\text{VO})_2\text{P}_2\text{O}_7$ crystal structure among the VPOr catalysts.

Regarding the stability of the catalysts, since the furfural conversion and MA yield returned to the initial level when the reaction temperature was increased to the highest value, no significant deactivation was detected for all of the studied catalysts (Fig. S4). The slight difference evidenced on furfural conversion between the initial and final segments at 320°C is due the steady state is not yet reached when the temperature change to 280°C .

Figure 5 shows the effect of the P/V molar ratio on the MA yield for the VPAq and VPOr catalysts. On *n*-butane oxidation to MA the crystalline $(\text{VO})_2\text{P}_2\text{O}_7$ phase is not only the active phase for the oxidation reaction but also selective in producing MA from *n*-butane partial oxidation³⁴. Therefore, in the VPOr catalysts, the preferentially exposed plane (200) of the $(\text{VO})_2\text{P}_2\text{O}_7$ phase (Fig. 2b), which is absent in the VPAq catalysts (Fig. 2a), could be responsible for the MA formation from furfural. The results shown in Figure 5b

experimentally confirm this, since the highest MA yields are obtained over VPOr with the best defined $(\text{VO})_2\text{P}_2\text{O}_7$ crystalline structure (VPOr_{0.43}) as the reaction temperature increases. The fact that (200) plane favors MA formation from furfural partial oxidation has been observed by Li et al. who prepared plate V-P-O catalysts⁵⁹.

A quick comparison between temperature extremes over catalysts with molar ratio $P/V=1$ is evidence of this. At 320°C the furfural conversion over VPOr_{1.0} almost doubles the conversion over VPAq_{1.0} (33% vs 17%, respectively), while the MA yield is more than 20% higher for VPOr_{1.0} with respect to VPAq_{1.0} at the same reaction conditions (9.7% vs 8%, respectively). At 280°C VPAq_{1.0} is not able to significantly oxidize furfural, however VPOr_{1.0} presents a furfural conversion of 8.2% reaching an MA yield of 1.1%.

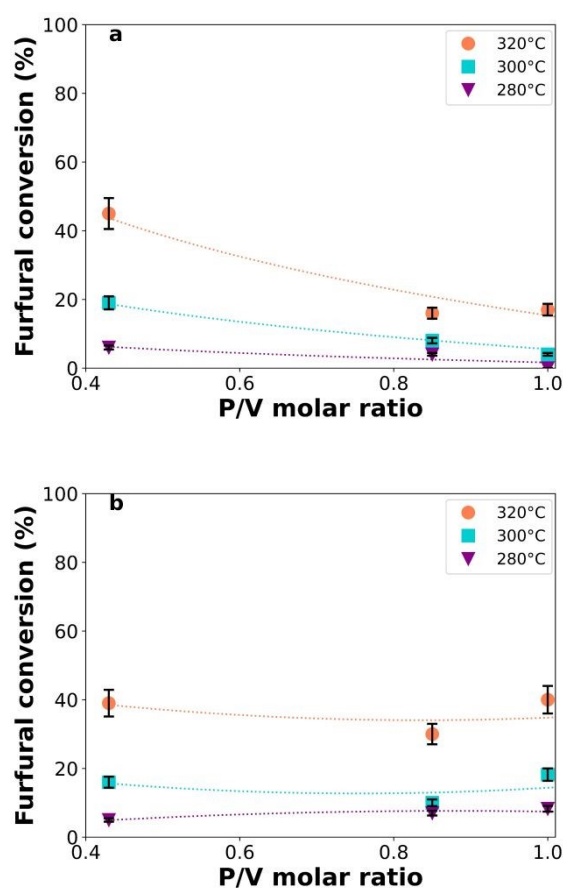


Figure 4. Furfural conversion vs. P/V molar ratio (0.43, 0.85, 1.00) at different reaction temperatures of 280°C , 300°C and 320°C on (a) VPAq and (b) VPOr catalysts. ($W/F=1.81$ min $\text{mg}_{\text{cat}} \text{mL}^{-1}$, $P_{\text{O}_2}/P_{\text{fur}}=20$). The lines are added to show the trend. Error bars indicate the standard deviation in furfural conversion (20%).

Influence of the reaction conditions on VPOr_{1.0} catalytic activity. Comparison with $\text{V}_2\text{O}_5/\text{Al}_2\text{O}_3$.

The kinetics of the reaction was studied by varying the $P_{\text{O}_2}/P_{\text{fur}}$ ratio in the feed as well as the space velocity. Since VPOr catalysts display

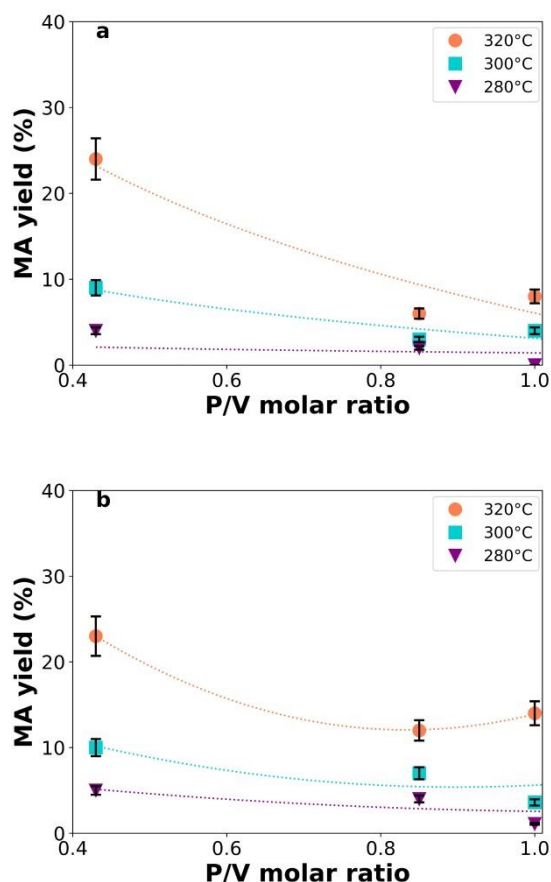


Figure 5. MA yield vs. P/V molar ratio at different reaction temperature on (a) VPAq and (b) VPOr catalysts. ($W/F=1.81 \text{ min mg}_{\text{cat}} \text{ ml}^{-1}$, $P_{\text{O}_2}/P_{\text{fur}}=20$). The lines are added to show the trend. Error bars indicate the standard deviation in MA yield (20%).

larger furfural conversion and MA yield compared with VPAq, the VPOr_{1.0} catalyst was chosen for the kinetics assays. It should be emphasized that the aim was the kinetics study of the furfural oxidation process instead of the optimization of the MA yield. The higher furfural conversion and MA yield of VPOr_{0.43} was not required in this case. Three $P_{\text{O}_2}/P_{\text{fur}}$ ratios were studied in the range of 280°C to 320°C (Fig. S5), and the CO₂ yield was included as an indication of total oxidation extent. Figure 6a shows that the furfural conversion and MA yield increase proportionally with the increase of the $P_{\text{O}_2}/P_{\text{fur}}$ ratio at 300°C, evidencing the importance of reactions R. 1 and R. 2. The MA yield did not decrease with the increase of the oxidizing potential, indicating that transformation of MA via total oxidation is not significant (R. 3). It is important to highlight that other products (not identified) were detected albeit in small amount. In this sense, the carbon balance was performed for the furfural partial oxidation in the whole range of reaction conditions. Over VPOr_{1.0}, the identified products and unconverted furfural detected at the reactor outlet accounted for 92.5% of the carbon in the inlet as average of all experiments. In the case of V₂O₅/Al₂O₃, the same compounds

accounted for 86.1% (Calculations detailed in section S2). This may be due to secondary reactions that polymerize the furfural, generating resin deposits on the surface of the catalysts. This has been observed on V₂O₅/Al₂O₃ and reported previously²⁷. Nevertheless, the activity of the catalysts was not significantly decreased during the 20h duration catalytic test. Longer run times may be required to determine if the polymerization affects the activity of the catalysts.

To evaluate the effect of the residence time, four W/F values were tested at different reaction temperatures, maintaining constant the inlet furfural partial pressure (Fig. S6). Figure 6b shows the W/F ratio influence at 300°C. CO₂ formation still almost constant with the increase in the W/F ratio, indicating that the total oxidation is not favored and the increase of furfural conversion is related to the increase of the MA yield. Furthermore, it implies that for VPOr_{1.0} catalyst, larger contact time favors MA formation without suffering subsequent oxidation or other side reactions.

The catalytic performance of the previously studied V₂O₅/Al₂O₃ catalyst was also analyzed. Figure 7a shows the effect of the $P_{\text{O}_2}/P_{\text{fur}}$ ratio and Figure 7b, the effect of W/F residence time on furfural conversion and MA and CO₂ yields at 300°C. The full temperature range is shown in Figure S6 for $P_{\text{O}_2}/P_{\text{fur}}$ ratio influence and in Figure S7 for W/F ratio influence. Compared to VPOr_{1.0} catalyst, it can be seen that, under the same experimental conditions, furfural conversion and MA yield tend to be higher for the V₂O₅/Al₂O₃ catalyst. This result could be attributed to the higher surface area, and hence a larger amount of surface V sites available on the V₂O₅/Al₂O₃ catalyst, compared to the bulk V-P-O catalysts. The increase in the MA yield with the increase of $P_{\text{O}_2}/P_{\text{fur}}$ ratio (Fig. 7a) is in line with previous reports^{27,71,72}, while the CO₂ yield shows the opposite trend. Figure 7b shows the effect of contact time on the furfural conversion and product yields. At higher temperatures (300°C and 320°C) the furfural conversion is almost complete. Under these conditions, the CO₂ yield and the MA yield each remain at a respective range, both with little change. Since that, the conversion does not change; this was expected for both yields.

Figure 8 shows the STY of MA as a function of the reaction temperature on V₂O₅/Al₂O₃ and bulk VPOr_{1.0} catalysts. Even though we evidenced a higher furfural conversion and MA yield on V₂O₅/Al₂O₃ catalyst, it is worth noting that under the stronger reaction condition i.e., 320°C and $P_{\text{O}_2}/P_{\text{fur}}=40$, the MA yield on V₂O₅/Al₂O₃ decreases, while on VPOr_{1.0} catalyst it keeps increasing. The combination of both effects, reaction temperature and $P_{\text{O}_2}/P_{\text{fur}}$ ratio defines the oxidative potential²⁷ as the conditions in which the catalyst exhibits its maximum oxidative performance and the maximum selectivity to MA production is reached. Although the V₂O₅/Al₂O₃ catalyst is inherently more active for oxidation reactions, under the same oxidative conditions, the complete furfural oxidation is favored. Figure 8 shows that the V₂O₅/Al₂O₃ catalyst presents the maximum performance at $P_{\text{O}_2}/P_{\text{fur}}=40$ and 280°C and that the VPOr_{1.0} catalyst does not reach the maximum MA yield during the experimental conditions. This result means that the VPOr_{1.0} catalyst requires higher oxidizing conditions ($T>320^\circ\text{C}$ and/or $P_{\text{O}_2}/P_{\text{fur}}>40$) to

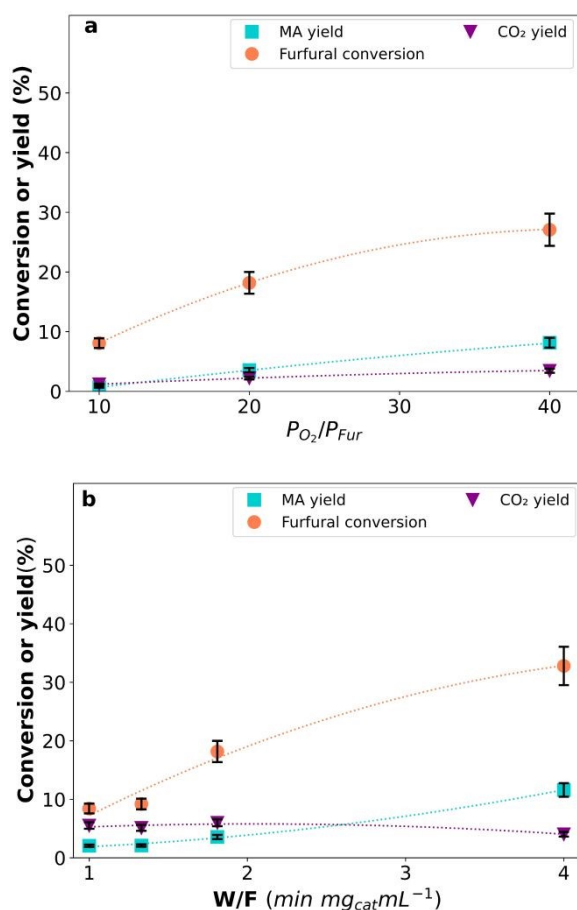


Figure 6. Effect of (a) the P_{O_2}/P_{fur} ratio at $300^\circ C$ on furfural conversion, MA yield, and CO_2 yield over $VPOr_{1.0}$ catalyst ($W/F=1.81$ $min\ mg_{cat}\ mL^{-1}$); (b) the W/F ratio at $300^\circ C$ on furfural conversion, MA yield and CO_2 yield over $VPOr_{1.0}$ catalyst ($P_{O_2}/P_{fur}=20$). The lines are added to show the trend. Error bars indicate the standard deviation in furfural conversion; MA and CO_2 yield (20%).

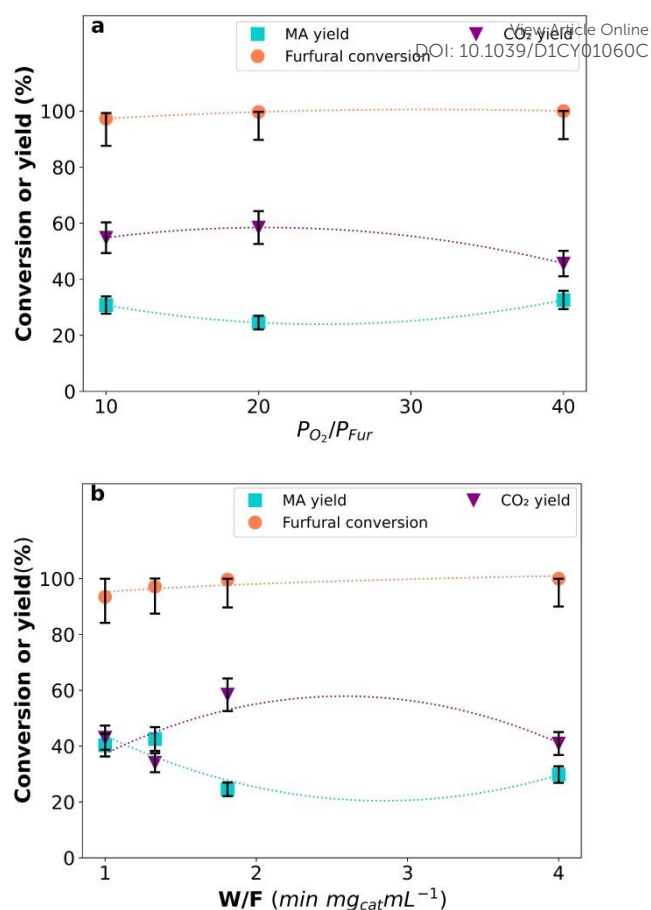


Figure 7. Effect of: (a) the P_{O_2}/P_{fur} ratio at $300^\circ C$ on furfural conversion, MA yield, and CO_2 yield over V_2O_5/Al_2O_3 catalyst ($W/F=1.81$ $min\ mg_{cat}\ mL^{-1}$); (b) the W/F ratio at $300^\circ C$ on furfural conversion, MA yield and CO_2 yield over V_2O_5/Al_2O_3 catalyst ($P_{O_2}/P_{fur}=20$). The lines are added to show the trend. Error bars indicate the standard deviation in furfural conversion, MA and CO_2 yield (20%).

achieve the same conversion than V_2O_5/Al_2O_3 catalyst.

A comparison with STY previously reported show similar trends. Li *et al.*⁵⁹ tested a V-P-O catalyst prepared by organic synthesis at $340^\circ C$ reaching $116\ g_{MA}kg_{cat}^{-1}h^{-1}$, which is the expected because the higher temperature used by these authors. In the same work, a V-P-O catalyst activated specially to reach a better defined $(VO)_2P_2O_7$ crystalline structure reach $234\ g_{MA}kg_{cat}^{-1}h^{-1}$ at the same temperature⁵⁹. In the case the V_2O_5/Al_2O_3 , others authors tested the furfural oxidation to MA between $300^\circ C$ and $345^\circ C$, reaching a maximum STY of $145\ g_{MA}kg_{cat}^{-1}h^{-1}$ at $315^\circ C$ ²⁷. Higher temperatures values cause a decrease in the MA selectivity with the minimum STY of $51.8\ g_{MA}kg_{cat}^{-1}h^{-1}$ at the upper temperature of the range studied²⁷.

Kinetic modelling of the partial oxidation of furfural

Previous studies reported by Fagúndez *et al.*²⁹ showed a first-order kinetics for both furfural and O_2 pressure on MA formation. Their results suggest that the reaction occur via a Langmuir-Hinshelwood

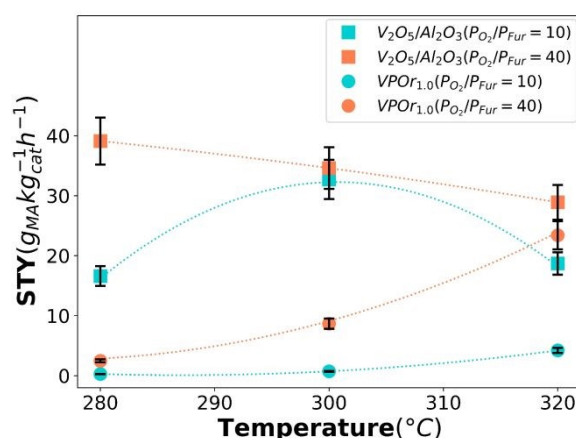


Figure 8. Effect of the reaction temperature on the STY for the supported V_2O_5/Al_2O_3 and bulk $VPOr_{1.0}$ catalysts at $280^\circ C$, $300^\circ C$ and $320^\circ C$. ($P_{O_2}/P_{fur}=10, 40$; $W/F=1.81$ $min\ mg_{cat}\ mL^{-1}$). The lines are added to show the trend.

mechanism. If the surface reaction between adsorbed furfural and oxygen is the rate determining step, one can derive equations 7a and 7b for furfural partial oxidation and furfural complete oxidation, respectively. It should be noted that the kinetic constants implicitly incorporate the kinetic constant of the rate determining step and the adsorption equilibrium constants of furfural and O₂ adsorption. The equations for partial and complete oxidation are thus the following:

$$-r_p = k_p P_{fur} P_{O_2} \quad (7a)$$

$$-r_c = k_c P_{fur} P_{O_2} \quad (7b)$$

Where k_c is the kinetic constant for complete oxidation (mol min⁻¹ g_{cat}⁻¹ kPa⁻²) and k_p is the kinetic constant for partial oxidation (mol min⁻¹ g_{cat}⁻¹ kPa⁻²)

The absence of adsorption terms in the denominator of equations 7a and 7b implies a negligible surface coverage by furfural, O₂, or their intermediates in the reactions. Furan and compounds with similar structure such as furanone has been identified as surface intermediates^{72,73}. Transient studies of furan, 2(5H)-furanone and MA adsorption over vanadyl pyrophosphate catalyst were carried out using FTIR spectroscopy and reported previously¹⁴. These authors inform a progressively coverage loss of all the compounds mentioned and their intermediates in a range of 200°C-300°C when the steady-state was reached (Experiment duration>3h). The clean surface observed under the mentioned temperature conditions are in line with equations 7a and 7b.

Partial oxidation and complete oxidation kinetic constants correspond to equations 8a and 8b, respectively. (Eq. 8a and Eq. 8b), the expressions were referred to the lower reaction temperature (280°C).

$$k_p = k_{p,280} e^{\left(\frac{E_{a,p}}{R} \left(\frac{1}{280} - \frac{1}{T}\right)\right)} \quad (8a)$$

$$k_c = k_{c,280} e^{\left(\frac{E_{a,c}}{R} \left(\frac{1}{280} - \frac{1}{T}\right)\right)} \quad (8b)$$

Where $E_{a,i}$ is the apparent activation energy (J mol⁻¹ K⁻¹), $k_{p,280}$ is the kinetic constant for partial oxidation at 280°C (mol min⁻¹ g_{cat}⁻¹ kPa⁻²), $k_{c,280}$ is the kinetic constant for complete oxidation at 280°C (mol min⁻¹ g_{cat}⁻¹ kPa⁻²), k_p is the kinetic constant for partial oxidation (mol min⁻¹ g_{cat}⁻¹ kPa⁻²), and k_c is the kinetic constant for complete oxidation (mol min⁻¹ g_{cat}⁻¹ kPa⁻²).

Table 4 summarizes the parameters required to fit the kinetic model and the average error of the model (ΣErr_{fur} and ΣErr_{MA}). The apparent activation energy for partial oxidation is higher than that for complete oxidation, which indicates that the former is favored at higher temperatures, as it has been shown in Figure 8 for the VPO_{1.0} catalyst. Schneider et al. reported an activation energy of 72.14 kJ/mol for the partial oxidation of *n*-butane to MA, and 72.02 kJ/mol for the complete oxidation to CO₂⁷⁴. Bej et al. reported slightly higher values (108 kJ/mol) for the partial oxidation of the same molecule⁷⁵.

Table 4. Parameters obtained from the Langmuir-Hinshelwood model for both catalysts (VPO_{1.0} and V₂O₅/Al₂O₃).

Catalyst	Reaction	k_{280} (mol min ⁻¹ g _{cat} ⁻¹ kPa ⁻²)*	E_{app} (kJ/mol)*	Mean error (%)	
				For P_{fur}	For P_{MA}
VPO _{1.0}	Furfural partial oxidation (R.1)	7.67±0.23×10 ⁻⁴	156±2.3	1.7	30.9
	Furfural complete oxidation (R.2)	4.66±0.05×10 ⁻³	90±0.9		
V ₂ O ₅ /Al ₂ O ₃	Furfural partial oxidation (R.1)	3.87±0.08×10 ⁻²	n.d.	17.6	10.4
	Furfural complete oxidation (R.2)	7.85±0.005×10 ⁻²	n.d.		
	MA complete oxidation (R.3)	4.19±0.42×10 ⁻⁶	n.d.		

*95% confidence interval calculated based on individual error.

The obtained apparent activation energy of 156 and 90 kJ/mol (Table 4), for the partial and complete oxidation, respectively, over the VPO_{1.0} catalyst are greater for both reactions; however, the molecule oxidized was different (*n*-butane vs furfural). The furfural molecule oxidation (partial or complete) require to break the furan ring demanding higher activation energy. Fagúndez et al.²⁷ reports a lower activation energy (98.3 kJ/mol) than the reported in this work, for furfural partial oxidation to MA over V₂O₅/γ-Al₂O₃. In this case, the catalyst used by these authors is quite more active than VPO_{1.0}

used here as was demonstrated previously in this document (Fig. 8). Then, the higher activity observed in the supported catalyst could be explained by this activation energy difference.

Figure S8 shows the parity plot for furfural partial pressure (Fig. S9a) and MA partial pressure (Fig. S9b) predictions. The model represent very accurately the experimental furfural partial pressure with a mean error of only 1.7%. On the other hand, the MA partial pressure present a higher average error, with a trend to under-predict the MA

ARTICLE

production. The fact that the kinetic models predict more accurately the reactant pressure than MA partial pressure, has been reported previously by Lorences for partial oxidation of *n*-butane¹⁵. This can be rationalized taking into account that MA errors are amplified by the fact that MA predictions also take into account the furfural prediction errors.

Figure 9 show the model fit at the extremes of the temperature work range as a function of the change in P_{O_2}/P_{fur} ratio (Fig. 9a) and W/F ratio (Fig. 9b). The kinetic model accurately predicts exit furfural partial pressure related with the P_{O_2}/P_{fur} ratio and the W/F ratio as well. MA yields are also accurately predicted although errors increase at the conditions where the experiments reach higher MA yields. These conditions are the extremes of the temperature (320°C), P_{O_2}/P_{fur} ratio (40) and W/F ratio (4 min/g_{cat} mL) work range. It could be argued that the assumptions made to propose the kinetic model begin to be less accurate, probably related to the occurrence of side reactions or the crowding of surface sites which the model does not predict. Future studies must be developed under similar experimental condition using techniques such as DRIFTS capable to determine the functional groups present on the catalyst surface during the reaction.

The developed reaction model was used to represent the experimental values obtained over V_2O_5/Al_2O_3 catalyst using the results at 280°C when the furfural conversion was not complete. In this case, the reaction *R.3* was included in the system since the decrease in the MA yield at higher furfural conversion indicated the occurrence of a consecutive path of complete MA oxidation (Fig. 8). A similar rate equation was used here (Eq. 9), namely assuming that surface reaction is the rate determining step and that the surface of the catalyst is empty.

$$-r_{cMA} = k_{cMA} P_{MA} P_{O_2} \quad (9)$$

The utilization of only one reaction temperature value prevents the obtaining of activation energies. However, it allowed to compare the kinetic constants for both $VPO_{r1.0}$ and V_2O_5/Al_2O_3 . Table 4 summarizes the kinetic constants for furfural partial and complete oxidation, as well as for MA complete oxidation, furthermore show the errors between the calculated and experimental partial pressures for both compounds.

The $k(V_2O_5/Al_2O_3):k(VPO_{r1.0})$ ratio for furfural partial oxidation indicate that the furfural partial oxidation is 50.5 times faster over the supported catalyst. Similarly, the furfural complete oxidation is 16.9 faster indicating that this catalyst favor the unselective oxidation as well.

Figure 10 represent the model fit to the experimental data obtained over the V_2O_5/Al_2O_3 catalyst at 280°C as a function of the change in P_{O_2}/P_{fur} ratio (Fig. 10a) and W/F ratio (Fig. 10b). The model was capable to represent the change in furfural and MA partial pressure as function of P_{O_2}/P_{fur} ratio and W/F ratio over this catalyst as well. Similarly to what happened with $VPO_{r1.0}$, the higher deviation occur at the extreme conditions evaluated where the assumptions made for propose the model become less accurate.

Catalysis Science & Technology

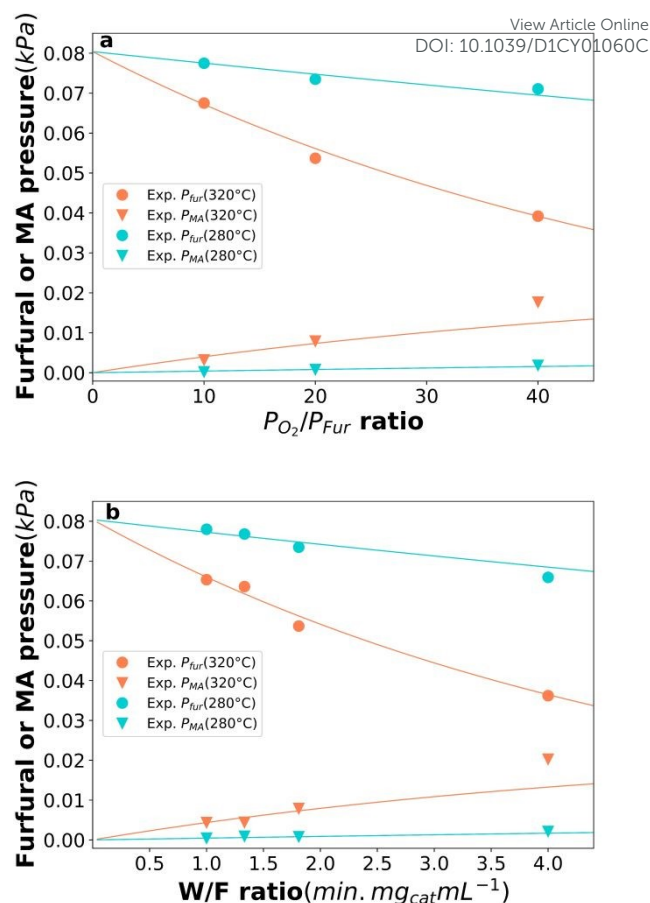


Figure 9. Model fit to the experimental data when occur a variation on (a) P_{O_2}/P_{fur} ratio ($W/F=1.81$ min mg_{cat} mL⁻¹) and (b) W/F ratio ($P_{O_2}/P_{fur}=20$) in the extremes of the temperature work range (280°C and 320°C), over $VPO_{r1.0}$. Lines correspond to model prediction for MA and furfural partial pressures at the exit of the reactor at 280°C and 320°C.

Conclusions

Two preparation methods, based on aqueous (VPAq) and organic (VPOr) media, were used to synthesize bulk vanadium phosphorous oxide (V-P-O) catalysts with different P/V molar ratios (0.43, 0.85, and 1.00). The preparation method exhibited a strong influence on the structure of the catalysts. VPOr catalysts present a more crystalline structure with a marked presence of crystalline $(VO)_2P_2O_5$ phase, considered responsible for the selective MA formation. On the other hand, an amorphous phase was detected in the VPAq catalysts, with a predominance of V(V), reported as a non-selective site for furfural partial oxidation to MA. The differences in the structure were reflected in the catalytic performance, being VPOr catalyst more selective for the partial oxidation of furfural to MA than VPAq catalysts. Both series of V-P-O catalysts were stable under the experimental conditions with no significant deactivation obser-

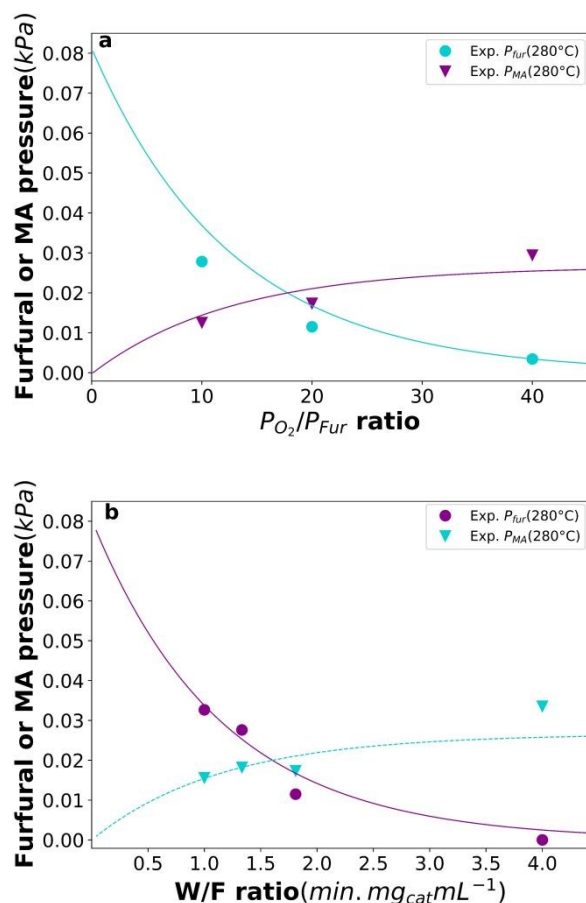


Figure 10. Model fit to the experimental data when occur a variation on (a) P_{O_2}/P_{Fur} ratio ($W/F=1.81 \text{ min } mg_{cat} mL^{-1}$) and (b) W/F ratio ($P_{O_2}/P_{Fur}=20$) at $280^\circ C$, over V_2O_5/Al_2O_3 . Lines correspond to model prediction for MA and furfural partial pressures at the exit of the reactor at $280^\circ C$.

ved. A higher P/V molar ratio led to a decrease in the specific surface area, particularly on VPAq. Besides, it causes a loss of crystallinity in the VPAq solids structure. In the VPOr catalysts, the increase in P/V ratio changes the crystallite size of $(VO)_2P_2O_5$ differently according to the plane ((200), (024), (032)), which means that the P/V ratio does not affect all planes equally. Future work should study lower P/V molar ratios in order to better understand the influence of this parameter on the selective oxidation of furfural.

Comparatively, a supported V_2O_5/Al_2O_3 catalyst was more active for furfural conversion (50.5 times faster than VPOr_{1.0} at $280^\circ C$), however, the selectivity decreased at higher reaction temperature and P_{O_2}/P_{Fur} ratios due to its also higher rates of total oxidation paths. On the contrary, the bulk VPOr_{1.0} catalyst showed a constant increase of activity and selectivity to MA at $320^\circ C$ and $P_{O_2}/P_{Fur}=40$. This result indicates that the bulk VPOr_{1.0} catalyst is stronger and more resistant to higher oxidizing potential with no significant loss in MA yield than the V_2O_5/Al_2O_3 catalyst. Kinetic modelling was used to estimate fundamental kinetic parameters for both, partial and complete furfural oxidation. The experimental data was fitted to a Langmuir-

Hinshelwood in which the rate determining step of both main reactions (partial and total oxidations) corresponds to the surface reaction of furfural and O_2 . The model accurately predicts the furfural consumption and MA production with a mean error of 16.3%. Moreover, the surface of the catalysts seems not to be occupied significantly by surface intermediates which is in line with previous reports. The apparent activation energy for furfural partial oxidation reaction is higher than for complete oxidation (156 kJ/mol vs 90 kJ/mol) which agrees with the increase in STY of MA at higher oxidizing potential for the studied V-P-O catalyst.

Conflicts of interest

There are no conflicts to declare.

Acknowledgements

CONICYT PIA/APOYO CCTE AFB170007 and ANID Millennium Science Initiative grant NCN17_040 are acknowledged for financing this work. Saint-Gobain NorPro is acknowledged for kindly providing the alumina support.

References

- 1 S. Shi, H. Guo and G. Yin, *Catal. Commun.*, 2011, **12**, 731–733.
- 2 X. Li, P. Jia and T. Wang, *ACS Catal.*, 2016, **6**, 7621–7640.
- 3 Y. Rodenas, R. Mariscal, J. L. G. Fierro, D. Martín Alonso, J. A. Dumesic and M. López Granados, *Green Chem.*, 2018, **20**, 2845–2856.
- 4 M. Müller, M. Kutscherauer, S. Böcklein, G. Mestl and T. Turek, *Chem. Eng. J.*, 2020, **401**, 126016.
- 5 M. Müller, M. Kutscherauer, S. Böcklein, G. Mestl and T. Turek, *Ind. Eng. Chem. Res.*, 2021, **60**, 218–229.
- 6 K. C. Waugh and Y. H. Taufiq-Yap, *Catal. Today*, 2003, **81**, 215–225.
- 7 G. S. Patience and M. J. Lorences, *Int. J. Chem. React. Eng.*, 2006, **4**, 1–18.
- 8 G. Busca, F. Cavani, G. Centi and F. Trifirò, *J. Catal.*, 1986, **99**, 400–414.
- 9 S. K. Bej and M. S. Rao, *Ind. Eng. Chem. Res.*, 1991, **30**, 1829–1832.
- 10 M. J. Lorences, G. S. Patience, R. Cenni, F. Díez and J. Coca, *Catal. Today*, 2006, **112**, 45–48.
- 11 S. K. Bej and M. S. Rao, *Ind. Eng. Chem. Res.*, 1991, **30**, 1819–1824.
- 12 S. K. Bej and M. S. Rao, *Appl. Catal. A, Gen.*, 1992, **83**, 149–163.
- 13 J. S. Buchanan and S. Sundaresan, *Appl. Catal.*, 1986, **26**, 211–226.
- 14 Z. Y. Xue and G. L. Schrader, *J. Catal.*, 1999, **184**, 87–104.
- 15 M. J. Lorences, G. S. Patience, F. V. Díez and J. Coca, *Ind. Eng. Chem. Res.*, 2003, **42**, 6730–6742.
- 16 J. Gascón, R. Valenciano, C. Téllez, J. Herguido and M. Menéndez, *Chem. Eng. Sci.*, 2006, **61**, 6385–6394.

- 17 R. Mariscal, P. Maireles-Torres, M. Ojeda, I. Sádaba and M. López Granados, *Energy Environ. Sci.*, 2016, **9**, 1144–1189.
- 18 N. R. Reed and E. S. C. Kwok, ed. P. B. T.-E. of T. (Third E. Wexler, Academic Press, Oxford, 2014, pp. 685–688.
- 19 G. Shen, B. Andrioletti and Y. Queneau, *Curr. Opin. Green Sustain. Chem.*, 2020, **26**, 100384.
- 20 P. L. Arias, J. A. Cecilia, I. Gandarias, J. Iglesias, M. López Granados, R. Mariscal, G. Morales, R. Moreno-Tost and P. Maireles-Torres, *Catal. Sci. Technol.*, 2020, **10**, 2721–2757.
- 21 N. Alonso-Fagúndez, I. Agirrezabal-Telleria, P. L. Arias, J. L. G. Fierro, R. Mariscal and M. L. Granados, *RSC Adv.*, 2014, **4**, 54960–54972.
- 22 A. C. Alba-Rubio, J. L. G. Fierro, L. León-Reina, R. Mariscal, J. A. Dumesic and M. López Granados, *Appl. Catal. B Environ.*, 2017, **202**, 269–280.
- 23 T. Soták, M. Hronec, M. Gál, E. Dobročka and J. Škriniarová, *Catal. Letters*, 2017, **147**, 2714–2723.
- 24 P. M. Malibo, P. R. Makgwane and P. G. Baker, *ChemistrySelect*, 2020, **5**, 6255–6267.
- 25 A. Hu, X. Wang, X. Wang, Q. Peng and H. Wang, *J. Theor. Comput. Chem.*, 2020, **19**, 1–13.
- 26 R. Gérardy, D. P. Debecker, J. Estager, P. Luis and J. C. M. Monbaliu, *Chem. Rev.*, 2020, **120**, 7219–7347.
- 27 N. Alonso-Fagúndez, M. Ojeda, R. Mariscal, J. L. G. Fierro and M. López Granados, *J. Catal.*, 2017, **348**, 265–275.
- 28 N. Pethan Rajan, G. S. Rao, V. Pavankumar and K. V. R. Chary, *Catal. Sci. Technol.*, 2014, **4**, 81–92.
- 29 N. Alonso-Fagúndez, M. L. Granados, R. Mariscal and M. Ojeda, *ChemSusChem*, 2012, **5**, 1984–1990.
- 30 F. Ivars-Barceló, G. J. Hutchings, J. K. Bartley, S. H. Taylor, P. Sutter, P. Amorós, R. Sanchis and B. Solsona, *J. Catal.*, 2017, **354**, 236–249.
- 31 P. Santander, L. Bravo, G. Pecchi and A. Karelavic, *Appl. Catal. A Gen.*, 2020, **595**, 117513.
- 32 B. M. Weckhuysen and D. E. Keller, *Catal. Today*, 2003, **78**, 25–46.
- 33 F. Ben Abdelouahab, R. Olier, N. Guilhaume, F. Lefebvre and J. C. Volta, *J. Catal.*, 1992, **134**, 151–167.
- 34 J. C. Volta, R. Olier, M. Roulet, F. B. Abdelouahab and K. Bere, *Stud. Surf. Sci. Catal.*, 1993, **75**, 1531–1534.
- 35 C. J. Kiely, A. Burrows, S. Sajji, G. J. Hutchings, M. T. Sananes, A. Tuel and J. C. Volta, *J. Catal.*, 1996, **162**, 31–47.
- 36 E. Bordes, *Catal. Today*, 1993, **16**, 27–38.
- 37 V. V. Gulians, J. B. Benziger, S. Sundaresan, I. E. Wachs, J. M. Jehng and J. E. Roberts, *Catal. Today*, 1996, **28**, 275–295.
- 38 M. Rezaei, A. Najafi Chermahini, H. A. Dabbagh, M. Saraji and A. Shahvar, *J. Environ. Chem. Eng.*, DOI:10.1016/j.jece.2018.102855.
- 39 L. M. Cornaglia and E. A. Lombardo, *Appl. Catal. A*, 1995, **127**, 125–138.
- 40 H. S. Horowitz, C. M. Blackstone, A. W. Sleight and G. Teufer, *Appl. Catal.*, 1988, **38**, 193–210.
- 41 N. P. Rajan, G. S. Rao, B. Putrakumar and K. V. R. Chary, *RSC Adv.*, 2014, **4**, 53419–53428.
- 42 Y. Zhang-Lin, M. Forissier, J. C. Volta and J. C. Védrine, *J. Catal.*, 1994, **145**, 267–275.
- 43 M. J. Lorences, G. S. Patience, F. V. Díez and J. Coca, *Appl. Catal. A Gen.*, 2004, **263**, 193–202. DOI: 10.1039/D1CY01060C
- 44 D. Wang and M. A. Barteau, *Appl. Catal. A Gen.*, 2002, **223**, 205–214.
- 45 M. S. Murthy and Rajamani, *Chem. Eng. Sci.*, 1974, **29**, 601–609.
- 46 K. Rajamani, P. Subramanian and M. S. Murthy, *Ind. Eng. Chem. Process Des. Dev.*, 1976, **15**, 232–234.
- 47 E. Bordes and P. Courtine, *J. Catal.*, 1979, **57**, 236–252.
- 48 B. Chen and E. J. Munson, *J. Am. Chem. Soc.*, 2002, **124**, 1638–1652.
- 49 F. Cavani, D. De Santi, S. Luciani, A. Löfberg, E. Bordes-Richard, C. Cortelli and R. Leanza, *Appl. Catal. A Gen.*, 2010, **376**, 66–75.
- 50 B. K. Hodnett, *Catal. Rev. - Sci. Eng.*, 1985, **3**, 373–424.
- 51 M. F. De Lange, T. J. H. Vlugt, J. Gascon and F. Kapteijn, *Microporous Mesoporous Mater.*, 2014, **200**, 199–215.
- 52 S. Brunauer, P. H. Emmett and E. Teller, *J. Am. Chem. Soc.*, 1938, **60**, 309–319.
- 53 E. P. Barrett, L. G. Joyner and P. P. Halenda, *J. Am. Chem. Soc.*, 1951, **73**, 373–380.
- 54 K. K. Unger, *Porous silica—Its properties and use as support in column liquid chromatography*, Elsevier Scientific Publishing Company, Amsterdam, 1st Editio., 1979, vol. 179.
- 55 H. Marsh and F. Rodríguez-Reinoso, *Activated Carbon*, Elsevier B.V, 1st edn., 2006.
- 56 M. Thommes, K. Kaneko, A. V. Neimark, J. P. Olivier, F. Rodríguez-Reinoso, J. Rouquerol and K. S. W. Sing, *Pure Appl. Chem.*, 2015, **87**, 1051–1069.
- 57 N. H. Batis, H. Batis, A. Ghorbel, J. C. Vedrine and J. C. Volta, *J. Catal.*, 1991, **128**, 248–263.
- 58 W. Weng, R. Al Otaibi, M. Alhumaimess, M. Conte, J. K. Bartley, N. F. Dummer, G. J. Hutchings and C. J. Kiely, *J. Mater. Chem.*, 2011, **21**, 16136–16146.
- 59 X. Li, J. Ko and Y. Zhang, *ChemSusChem*, 2018, **11**, 612–618.
- 60 A. Riaz, M. U. Ali, T. G. Enge, T. Tsuzuki, A. Lowe and W. Lipiński, *Research*, 2020, **2020**, 1–12.
- 61 K. Inumaru, M. Misono and T. Okuhara, *Appl. Catal. A Gen.*, 1997, **149**, 133–149.
- 62 G. Ertl, H. Knözinger, F. Schüth and J. Weitkamp, Eds., *Handbook of Heterogeneous Catalysis*, WILEY-VCH, Second., 2008.
- 63 Y. H. Taufiq-Yap, C. S. Yuen, N. Mohamed Nurul Suziana and R. Irmawati, *Cuihua Xuebao/Chinese J. Catal.*, 2014, **35**, 270–276.
- 64 A. Iglesias-Juez, M. V. Martínez-Huerta, E. Rojas-García, J. M. Jehng and M. A. Banares, *J. Phys. Chem. C*, 2018, **122**, 1197–1205.
- 65 Y. H. Taufiq-Yap, N. M. Nurul Suziana and M. Z. Hussein, *Catal. Letters*, 2011, **141**, 136–148.
- 66 A. A. Rownaghi, Y. H. Taufiq-Yap and F. Rezaei, *Catal. Letters*, 2009, **130**, 504–516.
- 67 L. Pérez-Moreno, S. Irusta, J. Soler, J. Herguido and M. Menéndez, *Chem. Eng. J.*, 2009, **147**, 330–335.
- 68 V. Mahdavi and H. R. Hasheminasab, *J. Taiwan Inst. Chem. Eng.*, 2015, **51**, 53–62.

- 69 X. Feng, Y. Yao, Q. Su, L. Zhao, W. Jiang, W. Ji and C. T. Au, *Appl. Catal. B Environ.*, 2015, **164**, 31–39.
- 70 A. Martin, C. Janke and V. N. Kalevaru, *Appl. Catal. A Gen.*, 2010, **376**, 13–18.
- 71 N. A. Milas and W. L. Walsh, *J. Am. Chem. Soc.*, 1935, **57**, 1388–1393.
- 72 V. A. Slavinskaya, D. R. Kreile, e. E. Dzilyuma and D. e. Sile, *Chem. Heterocycl. Compd.*, 1977, **13**, 710–721.
- 73 M. Rogojerov, G. Keresztury and B. Jordanov, *Spectrochim. Acta - Part A Mol. Biomol. Spectrosc.*, 2005, **61**, 1661–1670.
- 74 P. Schneider, G. Emig and H. Hofmann, *Ind. Eng. Chem. Res.*, 1987, **26**, 2236–2241.
- 75 S. K. Bej and M. S. Rao, *Ind. Eng. Chem. Res.*, 1991, **30**, 1824–1828.

View Article Online
DOI: 10.1039/D1CY01060C